

DC-cycleGAN: Bidirectional CT-to-MR Synthesis from Unpaired Data

Jiayuan Wang, *Graduate Student Member, IEEE*, Q. M. Jonathan Wu, *Senior Member, IEEE*, and Farhad Pourpanah, *Member, IEEE*.

Abstract—Magnetic resonance (MR) and computer tomography (CT) images are two typical types of medical images that provide mutually-complementary information for accurate clinical diagnosis and treatment. However, obtaining both images may be limited due to some considerations such as cost, radiation dose and modality missing. Recently, medical image synthesis has aroused gaining research interest to cope with this limitation. In this paper, we propose a bidirectional learning model, denoted as *dual contrast cycleGAN* (DC-cycleGAN), to synthesis medical images from unpaired data. Specifically, a *dual contrast* loss is introduced into the discriminators to indirectly build constraints between MR and CT images by taking the advantage of samples from the source domain as negative sample and enforce the synthetic images fall far away from the source domain. In addition, cross entropy and structural similarity index (SSIM) are integrated into the cycleGAN in order to consider both luminance and structure of samples when synthesizing images. The experimental results indicates that DC-cycleGAN is able to produce promising results as compared with other cycleGAN-based medical image synthesis methods such as cycleGAN, RegGAN, DualGAN and NiceGAN. The code will be available at <https://github.com/JiayuanWang-JW/DC-cycleGAN>.

Index Terms—Medical image synthesis, generative adversarial network, cycle consistency loss, magnetic resonance and computed tomography images.

I. INTRODUCTION

MAGNETIC resonance (MR) and computed tomography (CT) images are of great importance and widely used for diagnosis of various diseases such as cancer, as well as radiotherapy treatment planning [1]. On one hand, MR images are excellent in capturing the diversity of contrasts and accurately locating tumors and organs for structural images with soft tissues [2]. On the other hand, CT images are able to show details of the lesions and provide electron density information [3]. Since, unique information can be obtained from each modality, using both MR and CT images of the patients can dramatically improve clinical diagnosis and treatment. Nonetheless, some considerations, including cost, time, radiation dose and necessity of an accurate MR/CT registrations, may limit the acquisition of both images. These limitations can be avoided by synthesizing medical images from another modality, i.e., generating MR images from CT images [4].

Medical image synthesis can be defined as a mapping between target and source images. Existing methods can be grouped into feature mapping and deep learning (DL) methods. Feature mapping-based methods, which establish a mapping between similar patches of two modalities, can be further divided into atlas-, segmentation-, patch- and sparse coding-based methods [5]. As an example, atlas-based methods [6], first, measure the atlas-to-image transformation from source modality using the paired image atlases from both source and target modalities, and then use this transformation for generating images in the target modality. Feature mapping methods usually need many pre-/post-processing steps as well as a priory knowledge for tuning the transformation parameters. In addition, these methods face problems in generating low resolution images, and they are not able to produce variety of images with large anatomical differences [7].

In contrast, DL-based methods directly learn complex non-linear mappings from source domain to the target domain [8]–[11]. Convolutional neural networks (CNNs) [12] are among the most popular DL-based methods for medical image synthesis due to their ability in learning image structure. In [13], a CNN-based model is developed to generate positron emission tomography (PET) from MR images of the same subject. Nie et al. [14] generated CT images from MR images by adopting a 3D fully convolutional neural network (FCN). Fu et al. [15] used a U-Net structure to synthetic CT images from MR images. However, CNN-based models may generate blurred images due to a small voxel-wise misalignment of MR and CT images.

Recently, generative-based methods, including generative adversarial networks (GANs) [16] and Variational autoencoders (VAEs) [17], have shown remarkable results in synthesizing medical images of one modality conditioned on another modality [7], [18]–[20]. Nonetheless, these methods require a large number of paired images, i.e., both images are belong to the same patient, perfectly registered for training [21], which is difficult to obtain. In addition, if the registration has a local mismatch between different modalities, the learning models would generate irrelevant images. To overcome this issue, Zhu et al. [22] proposed cycleGAN to synthesize images from unpaired images in an unsupervised manner. However, cycleGAN can not be directly used to synthesize samples from another modality, i.e, MR-to-CT, as there are not direct constraints between MR and CT images [23]. To alleviate this, Zhang et al. [24] used an additional loss to force the

Manuscript received ; (Corresponding author: Q. M. Jonathan Wu)

J. Wang, Q. M. J. Wu and F. Pourpanah are with the Centre for Computer Vision and Deep Learning, Department of Electrical and Computer Engineering, University of Windsor, Windsor, ON N9B 3P4, Canada (e-mails: wang621@uwindsor.ca, jwu@uwindsor.ca and farhad.086@gmail.com).

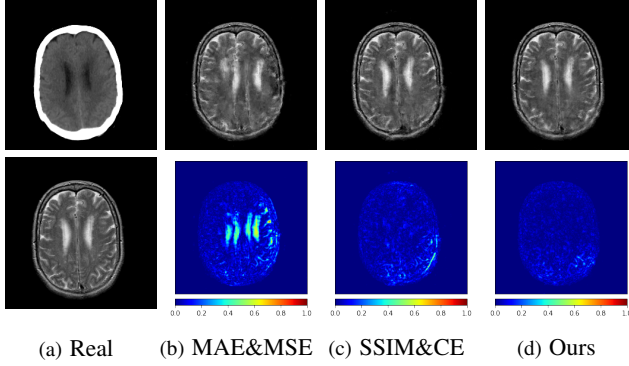


Fig. 1: Synthesized MR images along with errors between groundtruth and synthesized images by MAE & MSE, CE & SSIM without dual contrast loss and CE & SSIM with dual contrast losses (Ours). (a) shows the real images.

generated images to be the same as the real one. Later, SC-cycleGAN [23] defined a structure-consistency loss into the cycleGAN. Specifically, modality independent neighbourhood descriptor (MIND) [25] and a position-based selection strategy are used as structural features and slice selection, respectively. Moreover, several studies conducted bidirectional prediction, i.e., synthesis CT images from given MR images and synthesis MR images from CT images [5], [26].

In this paper, we propose a bidirectional learning model, known as *dual contrast cycleGAN (DC-cycleGAN)*, for medical image synthesis from unpaired data. Specifically, a dual contrast (DC) loss is formulated that leverages the advantage of samples from the source domain as negative samples to indirectly build constraints between MR and CT images via discriminators, and synthesize images more related to the source domain by enforcing the synthetic images to fall far away from the source domain. In addition, structural similarity index (SSIM) [27] and cross-entropy (CE) [28] are integrated into the DC-cycleGAN structure to avoid disappearing gradient information that is caused by mean absolute error (MAE) and synthesizing irrelevant images. SSIM considers luminance [27] and CE converges fast as its back-propagation error is less than MSE [29]. As can be seen in Figs. 1 and 2, using SSIM and CE with dual contrast can generate more clear and accurate MR images as compared with that of MAE and MSE, and SSIM and CE without dual contrast loss. Although both SSIM and CE with dual contrast and without dual contrast generate similar CT images, SSIM and CE with dual contrast quantitatively generate better images as shown in Table IV. The experimental results indicate that DC-cycleGAN is able to consider more complex features such as structure in synthesizing images and produce remarkable results as compared with other state-of-the-art methods reported in the literature.

The rest of the article is organized as follows. Section II presents the related work. The proposed bidirectional medical image synthesis model is presented in Section III. The experimental results and discussions are provided in Section IV. Finally, Section V concludes the paper and suggests future

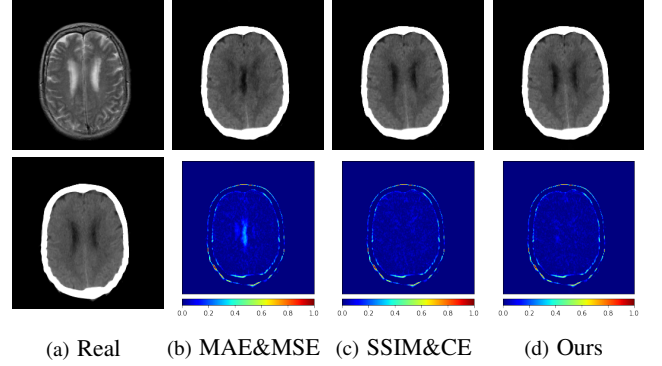


Fig. 2: Synthesized CT images along with errors between groundtruth and synthesized images by MAE & MSE, CE & SSIM without dual contrast loss and CE & SSIM with dual contrast losses (Ours). (a) shows the real images.

research directions.

II. RELATED WORKS

Synthesizing CT/MR images from another modality can significantly reduce the cost and help to accurately diagnose various diseases. However, it is a challenging issue to synthesize one modality from another one as there are no direct constraints between MR and CT images. In general, medical image synthesize methods can be trained either from paired data, i.e., aligned CT and MR images from the same patient, or unpaired data. In the following subsections we review these two categories.

A. Medical image synthesis using paired data

Most of the traditional medical image synthesis methods usually trained based on paired data. For example, a method based on multi-atlas registration and label propagation approach has been proposed to synthesize CT images from MR images in [30]. This method uses a pairwise registration technique to align the atlas MR and target images, and then generates CT images through a voxelwise atlas selection and intensity averaging. The proposed segmentation-based method proposed in [31] spatially aligns all MR volumes to the T1-weighted volume, then uses fuzzy c-means (FCM) clustering algorithm to compute the probability of belonging to a class for each voxel of images. Yang et al. [32] developed an approach that learns non-linear local descriptors and feature matching to generate CT images. This method projects linear descriptors into a nonlinear high-dimensional space to obtain non-linear descriptors. Then, it finds the nearest neighbours of local descriptor in the MR images to estimate CT patches.

Recently, with development of digital technologies, DL-based medical image synthesis methods have received more attention. Chen et al. [33] adopted a 2D-U-Net to synthesize CT slices from T2-weighted MR images. Nie et al. [34] integrated a 3D convolutional neural network (FCN) into the GAN structure to learn a mapping between CT and MR images. RU-ACGAN [35] combines ResNet, U-net and ACGAN [36]

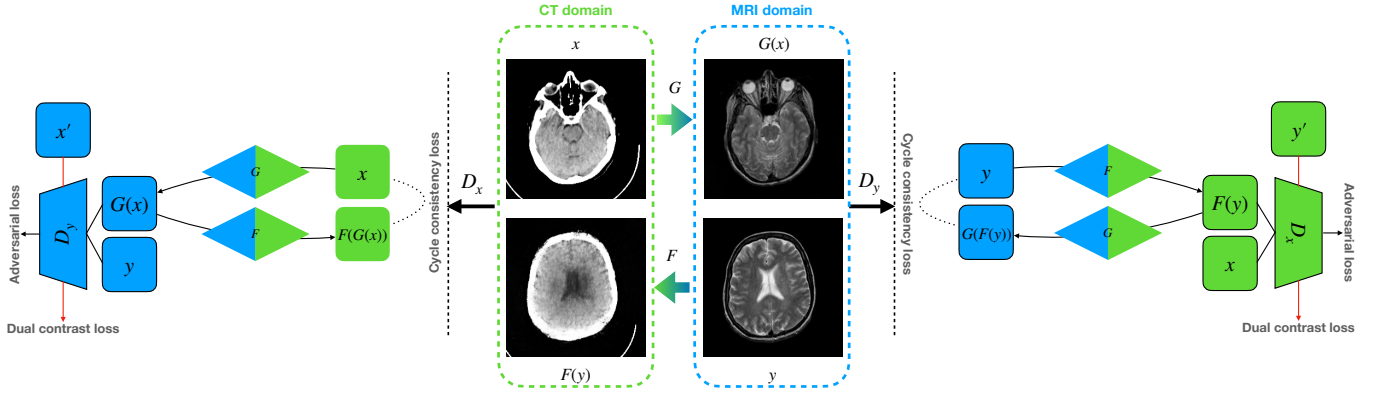


Fig. 3: The proposed DC-cycleGAN model for medical image synthesis from unpaired data. It receives real CT/MR images through generator to synthesis MR/CT images and discriminators distinguish real images from generated and real images from the source domain. Note that x' and y' are negative samples that are randomly selected from source images.

for CT estimation. Despite the success of these methods in synthesizing medical images from another modality, they require a large number of paired images, which is difficult in practice.

B. Medical image synthesis using unpaired data

To solve the problem of learning from paired data, unsupervised learning techniques have been developed that are able to learn from unpaired data. FedMed [37], which is a self-supervised learning method, generates brain images from unpaired data. A data augmentation technique is introduced for self-supervised learning and then feeds it into three auxiliary heads. Sohail et al. [38] used GAN for multi-contrast MR image synthesis from unpaired data. Specifically, star-GAN is used to translate given image into a number of contrasts, and then introduced a new loss function for generator to synthesize high-quality images. Chartsias et al. [39] synthesized MR images from CT images to improve segmentation of cardiac dataset.

Wolterink et al. [40] used a 2D cycleGAN to synthesis images from unpaired images. However, using 2D cycleGAN for constructing 3D volume may lead to observe spatial consistency in the generated images. Later, Zeng et al. [41] used a 3D FCNs as a generator to better model the spatial information and alleviate the discontinuity problem across slices. In [42], a cycleGAN with perceptual loss is used to train a model with weakly paired CT and MR images. Pseudo-3D cycleGAN [43] integrates neighbouring slices as well as cyclic loss function to ensure the consistency between MR and CT images. UagGAN [26] integrates unsupervised attention mechanism into GAN to improve the context misalignment problem during learning from unpaired data. Other studies that added additional losses into cycleGAN structure to synthesis high-quality images from unpaired data including cycleGAN with a shape consistency loss [24], cycleGAN with a gradient consistency loss [44], cycleGAN with adaptive instance normalization [45] and cycleGAN with structure-consistency loss [23], just to name a few. Inspired by the loss-correction,

RegGAN [46] trains generator with an additional registration network to adaptively fit the misaligned noise distribution.

In this study, we propose a bidirectional learning model based on cycleGAN to synthesis MR/CT images from unpaired data. Compared with other methods, our method uses the advantages of samples from source domain as negative samples during training to fall the synthesized images far away from the source domain and generate high-quality samples.

III. METHOD

In this section, we discuss the proposed DC-cycleGAN model in detail. First, an overview of DC-cycleGAN is provided, and then each component is discussed.

A. Model overview

In this section, we discuss our proposed DC-cycleGAN model for medical image synthesis in detail. The aim is to learn a bidirectional mapping function between MR and CT images using unpaired data, i.e., using MR and CT images from different subjects. Assume $X = \{x_i\}_{i=1}^N$ and $Y = \{y_j\}_{j=1}^M$ indicate sets of CT and MR images, respectively, where $x_i \in X$ and $y_i \in Y$. Similar to the cycleGAN, our DC-cycleGAN model (see Fig. 3) consists of two generators $G : x \rightarrow \hat{y}$ and $F : y \rightarrow \hat{x}$ for learning CT-to-MR and MR-to-CT mappings, respectively, where $\hat{y} = G(x)$ and $\hat{x} = F(y)$ represent synthesized MR and CT images, and two discriminators D_Y and D_X for distinguishing real MR and CT images from the synthetic or negative ones, respectively. In other word, the discriminators aim to distinguish whether the input image belongs to class 1, i.e., real image, or class 0, i.e., synthesized image or a sample from source domain. In addition, each discriminator includes a DC loss that leverage the advantages of samples from source domain as negative samples to enforce the synthesized images fall far away from the source domain.

B. CycleGAN

GAN [16] consists of a generator G and discriminator D_Y . The generator learns a mapping function $G : X \rightarrow Y$ to

map the source domain X to the target domain Y , while the discriminator computes the probability that a sample x belongs to the training data rather than synthesised one. D_Y and G are optimized by playing a minmax game, as follows:

$$\mathcal{L}_{\text{GAN}}(G, D_Y, X, Y) = \mathbb{E}_{y \sim p_{\text{data}}(y)} [\log D_Y(y)] + \mathbb{E}_{x \sim p_{\text{data}}(x)} [\log (1 - D_Y(G(x)))] . \quad (1)$$

Since the original GAN learns a mapping to produce outputs identically distributed in the target domain, it can map a given input to any random space in the target domain. Thus, GAN's training loss can not guarantee producing a desired output for a given input. One possible solution for this issue is to reconstruct back the synthesised samples into the source domain using a cycle consistency loss [22]. This requires to train a generator $F: Y \rightarrow X$ for reconstructing real samples and a discriminator D_X for distinguishing real images from the generated ones. The cycle consistency loss can be written as:

$$\mathcal{L}_{\text{cycle}}(G, F) = \mathbb{E}_{x \sim p_{\text{data}}(x)} [\|F(G(x)) - x\|_1] + \mathbb{E}_{y \sim p_{\text{data}}(y)} [\|G(F(y)) - y\|_1] . \quad (2)$$

The objective function for cycleGAN can be written as:

$$\mathcal{L}(G, F, D_X, D_Y) = \mathcal{L}_{\text{GAN}}(G, D_Y, X, Y) + \mathcal{L}_{\text{GAN}}(F, D_X, Y, X) + \lambda \mathcal{L}_{\text{cycle}}(G, F), \quad (3)$$

where λ is the weight between the two-loss functions.

However, Directly applying cycleGAN to synthesize samples from another modality, i.e., MR-to-CT, cannot generate high-quality images as there are not direct constraints between MR and CT images [23]. In other words, using adversarial and cycle consistency losses cannot guide the generator to learn a robust mapping in the target domain. To address this issue, in this study, we leverage the advantage of samples from the source domain as negative samples during training of discriminators. To achieve this, the concept of dual contrast is used, which is discussed in the next subsection.

C. Dual contrast

The original discriminator D_Y aims to distinguish the real images in target domain y from the synthesized images by the generator $G(x)$. Although using these images helps the generator to learn features from the Y domain, it can easily fool the discriminator by slightly changing some features of the samples from the source domain to the target domain, i.e., discriminator identifies the synthesized image as a real one. Thus, the generator $G(x)$ cannot learn a proper mapping in the target domain. To alleviate this issue, as shown in Fig. 4, we add an additional term, called *dual contrast* (D_c), to leverage the advantage of samples from the source domain x' (see Fig. 4), as follows:

$$\mathcal{L}_{\text{DC}}(D_Y, X, Y) = \mathbb{E}_{x' \sim p_{\text{data}}(x')} [\log(1 - D_Y(x'))] . \quad (4)$$

In this case, real images are considered as class 1 and both synthesized images and samples from source domain are considered as class 0. Thus, the discriminator's goal in our

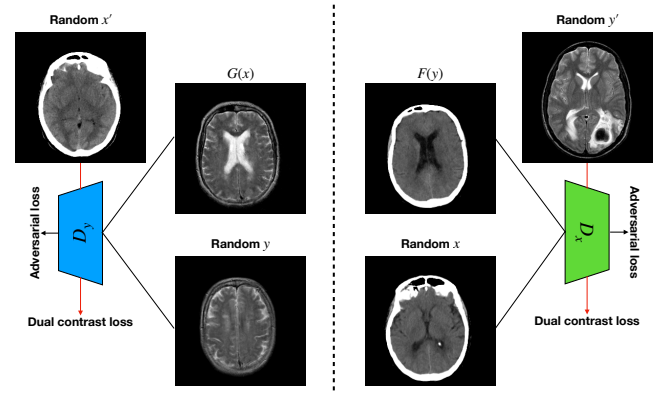


Fig. 4: The structure of proposed dual contrast. It adds negative samples, which are randomly selected, from the source domain to avoid mapping current samples close to the negative samples in the latent space.

proposed method is to distinguish whether the input image belongs to class 1, i.e., real image, or class 0, i.e., synthesized image or a sample from source domain. Adding images from source domain as negative samples forces the discriminator to guide the generator to synthesize image far away from the source domain in the latent space.

D. Training losses

CycleGAN uses mean squared error (MSE) in its structure to calculate the losses for discriminators, and mean absolute error (MAE) for generators. However, using MAE or MSE may lead to synthesize blurry images that cannot obtain human judgements of quality [47]. Besides, the gradient of MSE tends to disappear when it is used in the output layer of neural networks [28], and CE converges fast as its back-propagation error is less than MSE [29]. To overcome these issues, in this study, the cross-entropy (CE) and structural similarity index (SSIM) [27] are used instead of MSE and MAE, respectively.

1) *Cross entropy*: The main principle behind the CE is to transform the original optimization problem into a stochastic one, and then solve it by an adaptive random sampling algorithm [48]. It computes the difference, i.e., distance, between two distributions. CE is a common loss function that has been widely used for classification algorithms. In this study, the CE loss is integrated into the discriminators. Specifically, the PatchGAN's [49] discriminator is adopted, where the input to the discriminators can be either a real image from target domain, synthetic image or a randomly selected image from source domain. For a binary classification problem, the CE loss with sigmoid activation function can be defined as:

$$CE(t, y) = -\frac{1}{N} \sum_{i=1}^N t_i \cdot \log(y_i) + (1 - t_i) \cdot \log(1 - y_i), \quad (5)$$

where N is 256 because of 16×16 patches, t_i and y_i indicate the label and the predicted probability of the i -th patch, respectively.

2) *Structural similarity index*: (SSIM) [27] is an index that can be used to: (i) measure the similarity between two images, e.g., x_1 and x_2 , and (ii) evaluate the quality of an image. SSIM, first, normalizes data and then applies a Gaussian filter to each pixel of an image. Therefore, using SSIM can significantly improve the quality of the re-constructed image from another modality in presence of noise as compared with that of MAE [47]. SSIM considers luminance l , contrast c and structure s , and defined as follows:

$$SSIM(x_1, x_2) = \frac{(2\mu_{x_1}\mu_{x_2} + c_1)(2\sigma_{x_1x_2} + c_2)}{(\mu_{x_1}^2 + \mu_{x_2}^2 + c_1)(\sigma_{x_1}^2 + \sigma_{x_2}^2 + c_2)}, \quad (6)$$

where μ_{x_i} and σ_{x_i} are the mean value and standard deviation of i -th image ($i = 1, 2$), respectively, $\sigma_{x_1x_2}$ is the covariance of x_1 and x_2 . c_1 , c_2 and c_3 are constant values, where $c_3 = \frac{c_2}{2}$. In addition, l , c and s can be calculated as follows:

$$l(x_1, x_2) = \frac{2\mu_{x_1}\mu_{x_2} + c_1}{\mu_{x_1}^2 + \mu_{x_2}^2 + c_1}, \quad (7)$$

$$c(x_1, x_2) = \frac{2\sigma_{x_1}\sigma_{x_2} + c_2}{\sigma_{x_1}^2 + \sigma_{x_2}^2 + c_2}, \quad (8)$$

$$s(x_1, x_2) = \frac{\sigma_{x_1x_2} + c_3}{\sigma_{x_1}\sigma_{x_2} + c_3}. \quad (9)$$

In this study, the SSIM is used for two purposes. First, it is integrated into the generator to synthesis high-quality images from another modality. Second, it is used as an evaluation metric to compute the quality of the generated images.

Finally, by integrating SSIM into the cycle consistency loss, the resulting loss $\mathcal{L}_{\text{scycle}}$ can be written as follows:

$$\mathcal{L}_{\text{scycle}}(G, F) = SSIM(F(G(x)), x) + SSIM(G(F(y)), y). \quad (10)$$

E. Final objective function

In this study, the real images from X domain are added as negative samples in D_Y and the real images from Y domain are added as negative samples in D_X . The final objective function can be written as:

$$\begin{aligned} \mathcal{L}(G, F, D_X, D_Y) = & \mathcal{L}_{\text{GAN}}(G, D_Y, X, Y) + \\ & \mathcal{L}_{\text{GAN}}(F, D_X, Y, X) + \beta \mathcal{L}_{\text{DC}}(D_Y, X, Y) + \\ & \beta \mathcal{L}_{\text{DC}}(D_X, Y, X) + \lambda \mathcal{L}_{\text{scycle}}(G, F), \end{aligned} \quad (11)$$

where λ and β control the weights of cycle consistency and DC losses, respectively. The goal is to optimize:

$$G^*, F^* = \arg \min_{G, F} \max_{D_X, D_Y} \mathcal{L}(G, F, D_X, D_Y). \quad (12)$$

IV. EXPERIMENTS

This section evaluates the effectiveness of the proposed DC-cycleGAN model in generating images, i.e., MR from CT or CT from MR, from unpaired data, and compares its performance with other state-of-the-art methods such as cycleGAN [22], RegGAN [46], NICE-GAN [50], and Dual-GAN [51]. In addition, an ablation study is conducted to show

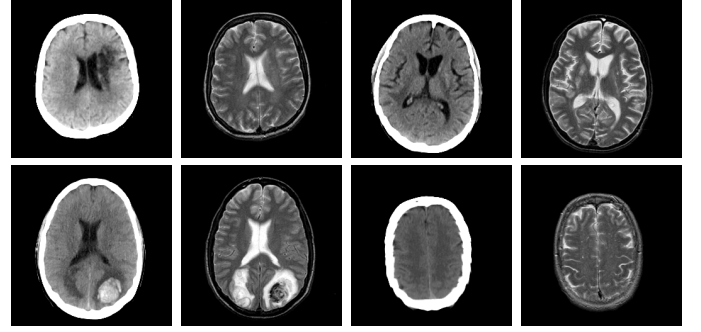


Fig. 5: Four randomly paired data were selected after pre-processing. As can be seen, head frames from CT images and noise from both CT and MR images are removed.

the effects of using negative samples in synthesizing medical images from other modality. In the following subsections, we first present dataset and evaluation metrics and implementation details, then the experimental results along with an ablation study are presented.

A. Dataset and evaluation metrics

1) *Dataset*: In this study, the dataset introduced in [52], which is publicly available¹, is used for performance evaluation. It consists of 367 paired CT and MR images with the size of 512×256. In the original dataset, it is noted that several CT images have stereotactic head frame that was used in Gamma Knife treatment. This head frame manually removed from the CT images. In addition, there exist various CT and MR slices that brings incredible difficulty in training the generator. Therefore, 100 images are selected from similar slices for each modality, in which 90 and 10 images are used for training and testing, respectively. Fig. 5 shows four examples of pre-processed samples.

2) *Evaluation metrics*: Three performance indicators, including SSIM, mean absolute error (MAE) and peak signal-to-noise ratio (PSNR), are used for performance evaluation and comparison. Among them, SSIM is formulated in subsection III-D2. MAE computes the average absolute between synthetic and real images. It can also be understood as the distance between two pictures. Defined as:

$$MAE = \frac{1}{MN} \sum_{i=1}^M \sum_{j=1}^N |x_1(i, j) - x_2(i, j)|, \quad (13)$$

where M and N are high and wide of image, respectively.

PSNR is another performance indicator for image quality assessment that can be computed as follows:

$$PSNR = 10 \log_{10}(L/MSE), \quad (14)$$

where L is dynamic range of the pixel values, and:

$$MSE = \frac{1}{MN} \sum_{i=1}^M \sum_{j=1}^N (x_1(i, j) - x_2(i, j))^2. \quad (15)$$

¹<https://github.com/ChengBinJin/MRI-to-CT-DCNN-TensorFlow>

TABLE I: MR synthesis quality evaluation metrics “Mean (standard deviation)” for various methods.

Method	MAE	PSNR	SSIM
RegGAN [46]	0.16828 (0.14436)	18.66927 (7.14952)	0.68031 (0.14813)
CycleGAN [22]	0.09155 (0.02325)	20.63825 (2.28951)	0.71670 (0.04504)
NICE-GAN [50]	0.08148 (0.00184)	21.44107 (0.21873)	0.70288 (0.00579)
DualGAN [51]	0.08038 (0.03109)	22.84981 (3.83697)	0.74028 (0.08261)
DC-cycleGAN	0.04559 (0.00333)	26.68858 (0.82837)	0.82622 (0.01220)

TABLE II: CT synthesis quality evaluation metrics “Mean (standard deviation)” for various methods.

Method	MAE	PSNR	SSIM
RegGAN [46]	0.04741 (0.00406)	19.88008 (0.63692)	0.81250 (0.00678)
CycleGAN [22]	0.05974 (0.01193)	20.07402 (1.52217)	0.81600 (0.02008)
NICE-GAN [50]	0.08373 (0.00789)	17.03886 (0.56989)	0.78790 (0.01014)
DualGAN [51]	0.04890 (0.01515)	22.11585 (1.60191)	0.83658 (0.02182)
DC-cycleGAN	0.03483 (0.00377)	25.19949 (1.67149)	0.87035 (0.01210)

A large PSNR means the real and synthetic images are closer .

B. Implementation details

Following the same procedure in cycleGAN [22], the instance normalization [53] is used. The generator contains three convolutions and nine residual blocks for 256×256 and high-resolution images, two fractionally-strided convolutions with stride 0.5. PathGANs [49] is used as discriminator to identify whether 94×94 overlapping image patches are real or generated. DC-cycleGAN trains generator five-times and then trains discriminator one-time. The parameters of DC-cycleGAN are set to: $\lambda = 10$ and $\beta = 0.5$, and the number of epochs and batch sizes are set to 200 and 1, respectively. Note that to have a fair comparison with other methods, we followed the original cycleGAN for λ and set it to 10. In addition, an experiment is conducted to obtain the best value for β (see Subsection IV-D). These parameters are obtained after several trial-and-errors. The code of DC-cycleGAN is available online². While parameters of other methods are adopted from their references.

For each experiment, we randomly selected 90% and 10% of the samples for training and test. This procedure is repeated 10 times and the mean value is used as the final value. All images are normalized between -1 and 1, and resized to 256×256 . All experiments are conducted using a server with Intel(R) Xeon(R) E5-2650 CPU and Nvidia GTX 1080TI GPU.

C. Results comparison

In this section, a comprehensive comparison between our proposed DC-cycleGAN with other recently published methods is conducted. These methods include conventional cycleGAN [22], RegGAN [46], NICE-GAN [50] and DualGAN [51]. Their published codes^{3 4 5 6} are used to generate

TABLE III: Ablation study. MR synthesis quality evaluation metrics “Mean (standard deviation)” under different conditions. “(w)” and “(wo)” indicate with and without dual contrast, respectively.

Method	MAE	PSNR	SSIM
MAE & MSE (wo)	0.06850 (0.01598)	23.62560 (2.42909)	0.78583 (0.03267)
MAE & MSE (w)	0.06939 (0.01849)	23.79743 (2.92001)	0.78368 (0.03924)
SSIM & CE (wo)	0.05562 (0.01858)	25.53608 (2.01767)	0.80613 (0.03585)
SSIM & CE (w)	0.04559 (0.00333)	26.68858 (0.82837)	0.82622 (0.01220)

TABLE IV: Ablation study. CT synthesis quality evaluation metrics “Mean (standard deviation)” under different conditions. “(w)” and “(wo)” indicate with and without dual contrast, respectively.

Method	MAE	PSNR	SSIM
MAE&MSE (wo)	0.04172 (0.01401)	23.57607 (2.93920)	0.85799 (0.02542)
MAE&MSE (w)	0.03800 (0.00721)	24.24584 (2.34511)	0.86124 (0.01885)
SSIM&CE (wo)	0.03582 (0.00400)	24.42528 (2.12593)	0.86676 (0.01117)
SSIM&CE (w)	0.03483 (0.00377)	25.19949 (1.67149)	0.87035 (0.01210)

results using the same parameters in their corresponding references.

Tables I and II show the quantitative accuracies of various methods in generating CT and MR images, respectively. As can be seen, DC-cycleGAN outperforms other methods in terms of MAE, PSNR and SSIM. This is mainly due to the dual contrast loss that is integrated into the DC-cycleGAN structure.

Moreover, Figs. 6 and 7 show the synthesized MR and CT images along with the errors between the real and synthesized images by different methods, respectively. It can be seen that the synthesized images by DC-cycleGAN are more identical to the real ones as compared with other methods. This indicates that effectiveness of SSIM and CE along with dual contrast in synthesizing images. In addition, the error between the groundtruth and synthesized MR/CT images by DC-cycleGAN is relatively less as compared with other methods.

D. Ablation study and sensitivity analysis

This section conducts an ablation study to show the impacts of using dual contrast, SSIM and CE in the DC-cycleGAN structure. To achieve this, four scenarios are considered, including:

- MAE and MSE without dual contrast denoted as MAE & MSE (wo),
- MAE and MSE with dual contrast denoted as MAE & MSE (w),
- SSIM and CE without dual contrast denoted as SSIM & CE (wo), and
- SSIM and CE with dual contrast denoted as SSIM & CE (w).

Tables III and IV show the results of MR and CT synthesis, respectively. As can be seen, all components play vital role in both tables. SSIM & CE (w) performs significantly better than other losses in synthesizing MR images. This also can be seen visually in Fig. 1. In contrast, SSIM&CE (w) performs slightly better than SSIM&CE (wo) in synthesizing CT images, both generate more or less similar CT images (see Table IV).

²<https://github.com/JiayuanWang-JW/DC-cycleGAN>

³<https://github.com/simontomaskarlsson/CycleGAN-Keras>

⁴<https://github.com/kid-liet/reg-gan>

⁵<https://github.com/alpc91/NICE-GAN-pytorch>

⁶<https://github.com/duxingren14/DualGAN>

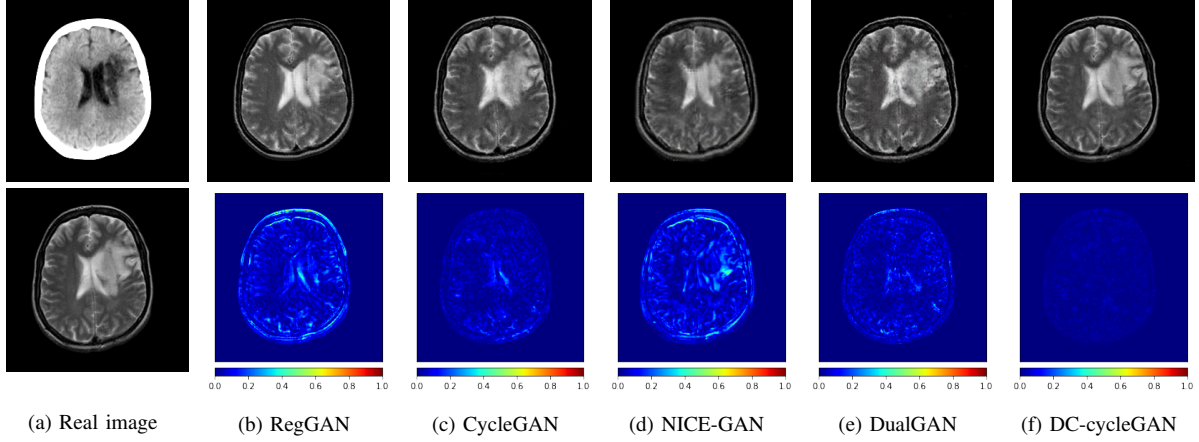


Fig. 6: Synthesized MR images along with errors between groundtruth and synthesized images by different methods. (a) shows the real images.

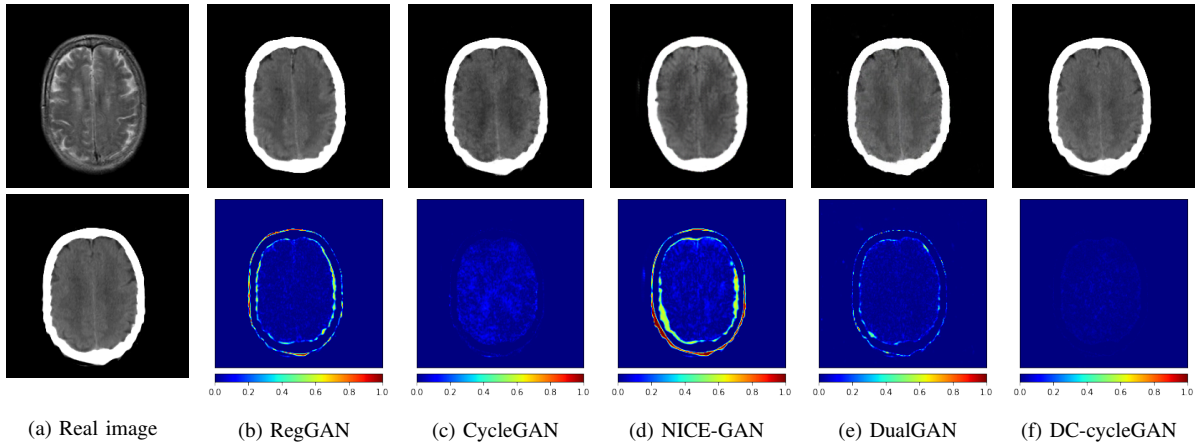


Fig. 7: Synthesized CT images along with errors between groundtruth and synthesized images by different methods. (a) shows the real images.

In addition, we have conducted an experiment to show the sensitivity of DC-cycleGAN to β . To achieve this, β is varied from 0.1 to 1. As shown in Fig. 8, the DC-cycleGAN produces the best results for both directions when β is set to 0.5.

V. CONCLUSION

In this study, the DC-cycleGAN model has been proposed for unsupervised medical image synthesis. It leverages the advantage of samples from the source domain as negative samples in learning a mapping between two image modalities using a dual contrast loss. It maps the learning samples far away from the images of the source domain. In addition, SSIM and CE losses are integrated into the DC-cycleGAN structure to consider both luminance and structure of samples. DC-cycleGAN is evaluated on brain MR-to-CT images and the results indicate that DC-cycleGAN is able to produce better CT/MR images in terms of both accuracy and visual quality as compared with state-of-the-art methods such as cycleGAN, RegGAN and dualGAN. Moreover, an ablation study is conducted to evaluate the impacts of different parts on

the performance. One limitation of this study is using images from one slice to train DC-cycleGAN and other methods, which is not realistic in practice. Our future work is focused on developing medical image synthesis models that are able to learn from datasets with multiple slices.

REFERENCES

- [1] B. Yueyun and L. Junping, "Analysis of the advantages and disadvantages of ct, mri and b ultrasound for their reasonable use," *Modern Hospital*, no. 1, pp. 62–63, 2008.
- [2] S. Mastrogiamaco, W. Dou, J. A. Jansen, and X. F. Walboomers, "Magnetic resonance imaging of hard tissues and hard tissue engineered bio-substitutes," *Molecular imaging and biology*, vol. 21, no. 6, pp. 1003–1019, 2019.
- [3] T. Wang, N. Manohar, Y. Lei, A. Dhakaan, H.-K. Shu, T. Liu, W. J. Curran, and X. Yang, "Mri-based treatment planning for brain stereotactic radiosurgery: dosimetric validation of a learning-based pseudo-ct generation method," *Medical Dosimetry*, vol. 44, no. 3, pp. 199–204, 2019.
- [4] D. Nie, R. Trullo, J. Lian, L. Wang, C. Petitjean, S. Ruan, Q. Wang, and D. Shen, "Medical image synthesis with deep convolutional adversarial networks," *IEEE Transactions on Biomedical Engineering*, vol. 65, no. 12, pp. 2720–2730, 2018.

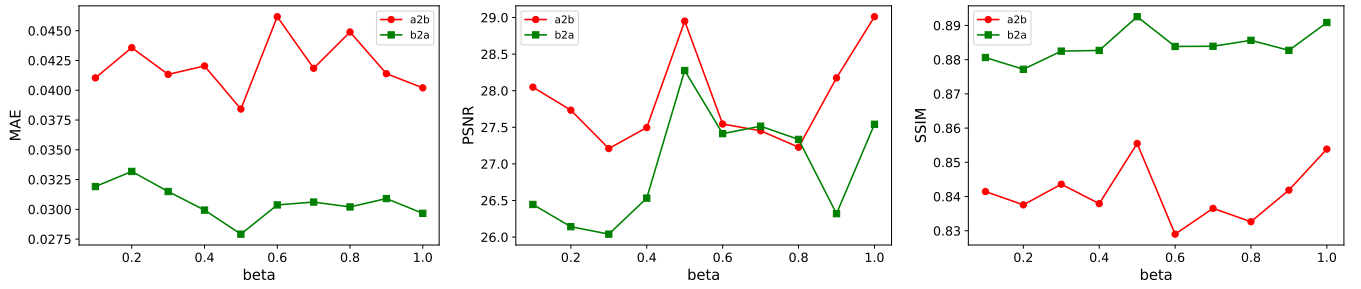


Fig. 8: The sensitivity analysis for β . “a2b” and “b2a” indicate CT-to-MR and MR-to-CT, respectively.

- [5] L. Xu, X. Zeng, H. Zhang, W. Li, J. Lei, and Z. Huang, “Bpgan: Bidirectional ct-to-mri prediction using multi-generative multi-adversarial nets with spectral normalization and localization,” *Neural Networks*, vol. 128, pp. 82–96, 2020.
- [6] B. Yu, L. Zhou, L. Wang, Y. Shi, J. Fripp, and P. Bourgeat, “Ea-gans: edge-aware generative adversarial networks for cross-modality mr image synthesis,” *IEEE transactions on medical imaging*, vol. 38, no. 7, pp. 1750–1762, 2019.
- [7] L. Bi, J. Kim, A. Kumar, D. Feng, and M. Fulham, “Synthesis of positron emission tomography (pet) images via multi-channel generative adversarial networks (gans),” in *molecular imaging, reconstruction and analysis of moving body organs, and stroke imaging and treatment*, 2017, pp. 43–51.
- [8] X. Zhou, H. Liu, F. Pourpanah, T. Zeng, and X. Wang, “A survey on epistemic (model) uncertainty in supervised learning: Recent advances and applications,” *Neurocomputing*, 2021.
- [9] X. Wang, Y. Zhao, and F. Pourpanah, “Recent advances in deep learning,” pp. 747–750, 2020.
- [10] F. Pourpanah, M. Abdar, Y. Luo, X. Zhou, R. Wang, C. P. Lim, and X.-Z. Wang, “A review of generalized zero-shot learning methods,” *arXiv:2011.08641*, 2020.
- [11] B. Li, Y. Gou, S. Gu, J. Z. Liu, J. T. Zhou, and X. Peng, “You only look yourself: Unsupervised and untrained single image dehazing neural network,” *International Journal of Computer Vision*, vol. 129, no. 5, pp. 1754–1767, 2021.
- [12] A. Krizhevsky, I. Sutskever, and G. E. Hinton, “Imagenet classification with deep convolutional neural networks,” *Advances in neural information processing systems*, vol. 25, 2012.
- [13] R. Li, W. Zhang, H.-I. Suk, L. Wang, J. Li, D. Shen, and S. Ji, “Deep learning based imaging data completion for improved brain disease diagnosis,” in *International conference on medical image computing and computer-assisted intervention*, 2014, pp. 305–312.
- [14] D. Nie, X. Cao, Y. Gao, L. Wang, and D. Shen, “Estimating ct image from mri data using 3d fully convolutional networks,” in *Deep Learning and Data Labeling for Medical Applications*, 2016, pp. 170–178.
- [15] J. Fu, Y. Yang, K. Singhrao, D. Ruan, D. A. Low, and J. H. Lewis, “Male pelvic synthetic ct generation from t1-weighted mri using 2d and 3d convolutional neural networks,” *arXiv preprint arXiv:1803.00131*, 2018.
- [16] I. Goodfellow, J. Pouget-Abadie, M. Mirza, B. Xu, D. Warde-Farley, S. Ozair, A. Courville, and Y. Bengio, “Generative adversarial nets,” in *Advances in Neural Information Processing Systems*, 2014, pp. 2672–2680.
- [17] D. P. Kingma and M. Welling, “Auto-encoding variational bayes,” *arXiv preprint arXiv:1312.6114*, 2013.
- [18] H. Zhu, Y. Cheng, X. Peng, J. T. Zhou, Z. Kang, S. Lu, Z. Fang, L. Li, and J.-H. Lim, “Single-image dehazing via compositional adversarial network,” *IEEE Transactions on Cybernetics*, vol. 51, no. 2, pp. 829–838, 2019.
- [19] J. H. Lee, I. H. Han, D. H. Kim, S. Yu, I. S. Lee, Y. S. Song, S. Joo, C.-B. Jin, and H. Kim, “Spine computed tomography to magnetic resonance image synthesis using generative adversarial networks: a preliminary study,” *Journal of Korean Neurosurgical Society*, vol. 63, no. 3, p. 386, 2020.
- [20] D. Nie and D. Shen, “Adversarial confidence learning for medical image segmentation and synthesis,” *International journal of computer vision*, vol. 128, no. 10, pp. 2494–2513, 2020.
- [21] S. Roy, W.-T. Wang, A. Carass, J. L. Prince, J. A. Butman, and D. L. Pham, “Pet attenuation correction using synthetic ct from ultrashort echo-time mr imaging,” *Journal of Nuclear Medicine*, vol. 55, no. 12, pp. 2071–2077, 2014.
- [22] J.-Y. Zhu, T. Park, P. Isola, and A. A. Efros, “Unpaired image-to-image translation using cycle-consistent adversarial networks,” in *Proceedings of the IEEE international conference on computer vision*, 2017, pp. 2223–2232.
- [23] H. Yang, J. Sun, A. Carass, C. Zhao, J. Lee, J. L. Prince, and Z. Xu, “Unsupervised mr-to-ct synthesis using structure-constrained cyclegan,” *IEEE transactions on medical imaging*, vol. 39, no. 12, pp. 4249–4261, 2020.
- [24] Z. Zhang, L. Yang, and Y. Zheng, “Translating and segmenting multimodal medical volumes with cycle-and shape-consistency generative adversarial network,” in *Proceedings of the IEEE conference on computer vision and pattern Recognition*, 2018, pp. 9242–9251.
- [25] M. P. Heinrich, M. Jenkinson, M. Bhushan, T. Matin, F. V. Gleeson, M. Brady, and J. A. Schnabel, “Mind: Modality independent neighbourhood descriptor for multi-modal deformable registration,” *Medical image analysis*, vol. 16, no. 7, pp. 1423–1435, 2012.
- [26] A. Abu-Srhan, I. Almallahi, M. A. Abushariah, W. Mahafza, and O. S. Al-Kadi, “Paired-unpaired unsupervised attention guided gan with transfer learning for bidirectional brain mr-ct synthesis,” *Computers in Biology and Medicine*, vol. 136, p. 104763, 2021.
- [27] Z. Wang, A. C. Bovik, H. R. Sheikh, and E. P. Simoncelli, “Image quality assessment: from error visibility to structural similarity,” *IEEE transactions on image processing*, vol. 13, no. 4, pp. 600–612, 2004.
- [28] Y. Zhou, X. Wang, M. Zhang, J. Zhu, R. Zheng, and Q. Wu, “Mpce: a maximum probability based cross entropy loss function for neural network classification,” *IEEE Access*, vol. 7, pp. 146 331–146 341, 2019.
- [29] A. Sangari and W. Sethares, “Convergence analysis of two loss functions in soft-max regression,” *IEEE Transactions on Signal Processing*, vol. 64, no. 5, pp. 1280–1288, 2015.
- [30] I. Mérida, N. Costes, R. A. Heckemann, A. Drzezga, S. Förster, and A. Hammers, “Evaluation of several multi-atlas methods for pseudo-ct generation in brain mri-pet attenuation correction,” in *2015 IEEE 12th international symposium on biomedical imaging (ISBI)*. IEEE, 2015, pp. 1431–1434.
- [31] S.-H. Hsu, Y. Cao, K. Huang, M. Feng, and J. M. Balter, “Investigation of a method for generating synthetic ct models from mri scans of the head and neck for radiation therapy,” *Physics in Medicine & Biology*, vol. 58, no. 23, p. 8419, 2013.
- [32] W. Yang, L. Zhong, Y. Chen, L. Lin, Z. Lu, S. Liu, Y. Wu, Q. Feng, and W. Chen, “Predicting ct image from mri data through feature matching with learned nonlinear local descriptors,” *IEEE transactions on medical imaging*, vol. 37, no. 4, pp. 977–987, 2018.
- [33] S. Chen, A. Qin, D. Zhou, and D. Yan, “U-net-generated synthetic ct images for magnetic resonance imaging-only prostate intensity-modulated radiation therapy treatment planning,” *Medical physics*, vol. 45, no. 12, pp. 5659–5665, 2018.
- [34] D. Nie, R. Trullo, J. Lian, C. Petitjean, S. Ruan, Q. Wang, and D. Shen, “Medical image synthesis with context-aware generative adversarial networks,” in *International conference on medical image computing and computer-assisted intervention*. Springer, 2017, pp. 417–425.
- [35] Q. Pengjiang, K. Xu, T. Wang, Z. Qiankun, H. Yang, B. Atallah, Z. Junqing, T. Bryan, and M. R. F Jr, “Estimating ct from mr abdominal images using novel generative adversarial networks,” *Journal of Grid Computing*, vol. 18, no. 2, pp. 211–226, 2020.
- [36] A. Odena, C. Olah, and J. Shlens, “Conditional image synthesis with auxiliary classifier gans,” in *International conference on machine learning*. PMLR, 2017, pp. 2642–2651.

- [37] G. Xie, J. Wang, Y. Huang, Y. Zheng, F. Zheng, and Y. Jin, “Fedmed-atl: Misaligned unpaired brain image synthesis via affine transform loss,” *arXiv preprint arXiv:2201.12589*, 2022.
- [38] M. Sohail, M. N. Riaz, J. Wu, C. Long, and S. Li, “Unpaired multi-contrast mr image synthesis using generative adversarial networks,” in *International Workshop on Simulation and Synthesis in Medical Imaging*. Springer, 2019, pp. 22–31.
- [39] A. Chartsias, T. Joyce, R. Dharmakumar, and S. A. Tsiftaris, “Adversarial image synthesis for unpaired multi-modal cardiac data,” in *International workshop on simulation and synthesis in medical imaging*. Springer, 2017, pp. 3–13.
- [40] J. M. Wolterink, A. M. Dinkla, M. H. Savenije, P. R. Seevinck, C. A. van den Berg, and I. Išgum, “Deep mr to ct synthesis using unpaired data,” in *International workshop on simulation and synthesis in medical imaging*, 2017, pp. 14–23.
- [41] G. Zeng and G. Zheng, “Hybrid generative adversarial networks for deep mr to ct synthesis using unpaired data,” in *International Conference on Medical Image Computing and Computer-Assisted Intervention*, 2019, pp. 759–767.
- [42] S. K. Kang, H. J. An, H. Jin, J.-i. Kim, E. K. Chie, J. M. Park, and J. S. Lee, “Synthetic ct generation from weakly paired mr images using cycle-consistent gan for mr-guided radiotherapy,” *Biomedical Engineering Letters*, pp. 1–9, 2021.
- [43] R. Oulbacha and S. Kadoury, “Mri to ct synthesis of the lumbar spine from a pseudo-3d cycle gan,” in *2020 IEEE 17th international symposium on biomedical imaging (ISBI)*, 2020, pp. 1784–1787.
- [44] Y. Hiasa, Y. Otake, M. Takao, T. Matsuoka, K. Takashima, A. Carass, J. L. Prince, N. Sugano, and Y. Sato, “Cross-modality image synthesis from unpaired data using cyclegan,” in *International workshop on simulation and synthesis in medical imaging*. Springer, 2018, pp. 31–41.
- [45] S. Yang, E. Y. Kim, and J. C. Ye, “Continuous conversion of ct kernel using switchable cyclegan with adain,” *IEEE Transactions on Medical Imaging*, vol. 40, no. 11, pp. 3015–3029, 2021.
- [46] L. Kong, C. Lian, D. Huang, Y. Hu, Q. Zhou *et al.*, “Breaking the dilemma of medical image-to-image translation,” *Advances in Neural Information Processing Systems*, vol. 34, 2021.
- [47] J. Snell, K. Ridgeway, R. Liao, B. D. Roads, M. C. Mozer, and R. S. Zemel, “Learning to generate images with perceptual similarity metrics,” in *2017 IEEE International Conference on Image Processing (ICIP)*. IEEE, 2017, pp. 4277–4281.
- [48] S. Mannor, D. Peleg, and R. Rubinstein, “The cross entropy method for classification,” in *Proceedings of the 22nd international conference on Machine learning*, 2005, pp. 561–568.
- [49] P. Isola, J.-Y. Zhu, T. Zhou, and A. A. Efros, “Image-to-image translation with conditional adversarial networks,” in *Proceedings of the IEEE conference on computer vision and pattern recognition*, 2017, pp. 1125–1134.
- [50] R. Chen, W. Huang, B. Huang, F. Sun, and B. Fang, “Reusing discriminators for encoding: Towards unsupervised image-to-image translation,” in *Proceedings of the IEEE/CVF Conference on Computer Vision and Pattern Recognition*, 2020, pp. 8168–8177.
- [51] Z. Yi, H. Zhang, P. Tan, and M. Gong, “Dualgan: Unsupervised dual learning for image-to-image translation,” in *Proceedings of the IEEE international conference on computer vision*, 2017, pp. 2849–2857.
- [52] X. Han, “Mr-based synthetic ct generation using a deep convolutional neural network method,” *Medical physics*, vol. 44, no. 4, pp. 1408–1419, 2017.
- [53] D. Ulyanov, A. Vedaldi, and V. Lempitsky, “Instance normalization: The missing ingredient for fast stylization,” *arXiv preprint arXiv:1607.08022*, 2016.